Performance Characteristics of the Kennedy Space Center 50-MHz Doppler Radar Wind Profiler Using the Median Filter/First-Guess Data Reduction Algorithm

ROBIN S. SCHUMANN AND GREGORY E. TAYLOR

ENSCO, Inc., Cocoa Beach, Florida

FRANCIS J. MERCERET

NASA/Kennedy Space Center, Florida

TIMOTHY L. WILFONG

Science and Technology Corporation, Boulder, Colorado

ABSTRACT

The performance of an improved signal-processing algorithm implemented on the NASA 50-MHz radar wind profiler at Kennedy Space Center is analyzed. In 1990, NASA began using a 50-MHz Doppler radar wind profiler to demonstrate the applicability of the technology to assessing launch wind conditions at Kennedy Space Center. To produce critical wind profiles in minimal time, NASA replaced the conventional signal-processing system delivered by the manufacturer with a more robust system. The new signal-processing system uses a median filter to remove spurious Doppler spectral data and constrains the search for the atmospheric signal by a first guess. The new system has been in nearly continuous operation since mid-1994. Over this period, the system performance was evaluated in varied weather conditions, and numerous comparisons with wind profiles from radar-tracked jimspheres were accomplished. The system is now integrated into the prelaunch wind evaluation structure. This paper discusses the details of the new signal-processing system and presents the results of the performance analysis.

1. Introduction

In 1990, the National Aeronautic and Space Administration/Kennedy Space Center (NASA/KSC) installed a 50-MHz Doppler radar wind profiler (DRWP) to evaluate its applicability for measuring upper-level winds in support of space lift operations. The profiler has operated continuously since that time primarily in an evaluation and research mode. Operational measurements of upper-level winds are made using radar-tracked specialized balloons called jimspheres. The profiler wind measurements are used to assist in the quality control of the jimsphere-measured profiles and to detect rapidly occurring wind shifts between the last jimsphere release and the eventual vehicle launch.

The appendix in this paper contains a detailed description of the 50-MHz system and its operational configuration. At the time of its installation, the signal-processing algorithms used to derive the winds were much the same as those used by the Colorado profiler network (Strauch et al. 1984). From 1990 through 1993, the KSC 50-MHz profiler produced a single-cycle profile every 3 min and reported a 30-min consensus average to the data users. In this case, the consensus required a minimum of four measurements to be within 2 m s^{-1}.

From the time of its installation, the Marshall Space Flight Center (MFSC) began evaluating how the profiler could improve the wind velocity estimates used for prelaunch wind field evaluation. Though the consensus-averaging algorithm eliminated most transient interference signals, it was highly susceptible to persistent interference and often produced erroneous wind estimates. This was unacceptable for wind estimates flowing directly into vehicle stress computations. MSFC's approach to improving the quality of wind profiles produced by the profiler was to develop improvements that could be readily implemented in real time. In the case of the KSC wind profiler, the only data accessible for analysis and algorithm development were the averaged spectra. Thus, the MSFC algorithm development concentrated on the atmospheric signal identification portion of the signal processing.

Corresponding author address: Robin S. Schumann, ENSCO, Inc., 1980 N. Atlantic Ave., Suite 230, Cocoa Beach, FL 32931.
E-mail: rschumann@fl.ensco.com

MSFC proposed the median filter/first-guess (MFFG) algorithm (Wilfong et al. 1993) to obtain more accurate and higher temporal resolution wind estimates than were available from consensus averaging the original signal-processing algorithm results. This algorithm makes use of a temporal median filter to eliminate transient interference signals and uses a first-guess wind velocity to incorporate the wind's time continuity into an algorithm for selecting the wind signal within the frequency spectrum. For situations where the accuracy of the wind is critical such as prior to launch when the vehicle stresses due to winds and flight path must be determined, the MFFG algorithm is coupled with an interactive quality control methodology. In 1994, KSC installed the MFFG algorithm to improve the quality as well as increase the temporal resolution of the available wind profiles.

The MFFG algorithm was evaluated extensively prior to its real-time implementation on the KSC 50-MHz DRWP, and its performance since then has been monitored closely. In this paper we describe the NASA/KSC 50-MHz profiler and the MFFG algorithm used to identify the atmospheric signal and attempt to provide an accurate indication of their performance by summarizing the analyses performed thus far.

2. Background

In the mid- to late 1970s several demonstration research wind profilers were constructed to study the atmosphere as well as to demonstrate the feasibility of remote sensing of the wind velocities in the stratosphere and troposphere and even the mesosphere. As research instruments, these profilers, as described by Gage and Balsley (1978), exhibited several different antenna, transmitter, and radar configurations. In this period of profiler atmospheric research, the signal processing and quality control of the wind estimates were performed offline. In the early 1980s as the research emphasis moved more toward determining the most feasible hardware configuration for operational wind profiling (Balsley and Gage 1982), the signal-processing emphasis lay in the theoretical determination of the most efficient profiling hardware configuration and transmitting frequency.

As the feasibility of developing a radar system that could be used for operational wind profiling became less of an issue, attention was turned toward the problem of estimating the wind velocities from the radar data in real time. In the ideal case, the average Doppler shift is calculated by taking the weighted average of the entire power spectrum. In the ideal case, however, the power spectrum is not contaminated with other returns such as those by ground clutter. In those cases, special signal-processing techniques must be applied to remove the contribution of the interference prior to calculating the moments (Woodman 1985) or, in the case of precipitation interference analysis of double-peaked spectra, to infer information regarding both the wind velocity and the precipitation fall speed (Wakasugi et al. 1985).

In the Colorado profiler network, the effects of interference signals on the spectral moments were mitigated somewhat by limiting the integration of the power spectrum to an interval surrounding the maximum spectral power density. The endpoints of the interval are the first points on either side of the maximum at which the spectrum power density falls below the noise level (Strauch et al. 1984). When the maximum spectral power density was associated with the atmospheric signal, this method worked very well and was highly reliable even for low signal-to-noise ratios (SNRs). If, however, the maximum spectral power density spectral peak is associated with a signal other than the atmospheric signal, the resulting radial velocity estimate will be in error. In the Colorado profiler network the consensus average of 12 (this number is variable) consecutive velocity estimates was taken to eliminate outliers in the hourly reported radial velocities. Depending upon the end users' task (e.g., quality monitoring, short-term forecasting, etc.), consensus averages have been generated for shorter intervals provided there were sufficient single-cycle estimates produced within the consensus time interval. The interval's consensus average consisted of the average of the largest subset of the single-cycle radial velocity estimates measured during the interval that were within a predefined delta of each other. Consensus averaging was found to be an effective method for estimating the wind velocities even when the SNR was as low as -19 dB (after time domain integration) as long as interference did not overshadow the atmospheric signal (May and Strauch 1989).

The KSC 50-MHz profiler was installed in 1990 around the same time the first National Oceanic and Atmospheric Administration (NOAA) Wind Profiler Demonstration Network profiler (WPDN) was being evaluated. It was found that both the NASA 50-MHz and WPDN profilers produced good consensus profiles most of the time and that the profilers usually agreed with the then current method of measuring winds, rawinsondes, and jimspheres (specialized radar-tracked balloons). Differences between balloon- and profiler-measured winds were attributed to several factors including instrumentation noise, varying wind conditions over the time and space that the profilers and balloons are measuring the winds, and interference contaminating the estimates made by the wind profilers (Weber et al. 1990; Weber and Wuertz 1990).

During the years following the installations of the WPDN, considerable research progressed on signal-processing methods that would eliminate the effects of interference signals and improve the quality of the wind estimates. In addition to the MFFG algorithm presented here, several signal-processing methods that address the assumption that the maximum spectral power density is associated with the atmospheric signal have been implemented on research and operational profilers. During

the OK PRE_STORM campaign, Yoe and Larsen (1992) found it necessary to account for double-peaked spectra in their use of VHF profilers to examine air motions in a convective environment. During the Lake Ontario Winter Storms experiment Clothiaux et al. (1994) found that at each range gate of the 404-MHz profiler used for the experiment there were usually at least two peaks evident in the spectra: one due to persistent ground clutter that had a large amplitude and a velocity near zero and one or more peaks not associated with ground clutter. Often more than one peak was distinct from the ground clutter, making selection of the atmospheric signal nontrivial. For the purposes of analysis, the group was able to postprocess archived spectra and developed a feature-based algorithm that included neural network processing to determine the atmospheric wind profile for each radar cycle.

As seen by MSFC during their initial evaluation of the 50-MHz profiler, NOAA noted that the consensus averaging method of quality controlling the wind estimates occasionally produces erroneous or nonrepresentative wind profiles. While evaluating the Environmental Technology Laboratory (ETL; formerly the Wave Propagation Laboratory) Colorado profiler network, Weber and Wuertz (1991) developed an algorithm making use of height and time continuity to eliminate outliers from the radial velocity estimates, which performed better than consensus averaging alone. The Weber–Wuertz algorithm can be applied to the data at any timescale and has been implemented on the WPDN profilers to quality control the hourly consensus averaged profiles (Miller et al. 1994; Barth et al. 1994). NOAA/ETL's further research indicated that even when the consensus-averaged profiles are not contaminated by interference, they occasionally may not be representative of the true atmospheric conditions. During times of small-scale atmospheric disturbances, the vertical and horizontal velocities may vary from one antenna beam to the next and certainly over the time span the radial velocities are consensus averaged. The consensus averaging in these cases can miss significant changes or fail to produce a minimum consensus due to rapid changes over the averaging time (Weber et al. 1992; Weber et al. 1993).

The ramifications of the consensus-averaged wind profiles not being representative of the true atmospheric conditions are disastrous when the wind profiler is used in support of shuttle or other vehicle launches. The absence of five beams on the KSC 50-Mhz profiler makes it imperative that the highest time resolution wind estimates are examined to ensure that the wind profiles are representative of the true wind field. Little research has been done on the utility of high-temporal resolution wind profiles, although NOAA and others in the profiler community have suggested this as a promising area for further research (Wuertz et al. 1995). The 924-MHz profilers included in the Mobile Profiling System (Wolfe et al. 1995) use the Weber–Wuertz algorithm to quality

control each wind profile, and the data users can then average the profiles over any averaging period.

3. Median filter/first-guess algorithm

The typical signal-processing scenario for the NOAA and many other Doppler radar wind profilers involves the following discrete steps applied to each on a gate-by-gate basis:

1) sampling and time domain averaging,
2) DC removal,
3) windowing and power spectrum calculation,
4) spectral averaging,
5) ground clutter removal,
6) noise estimation,
7) atmospheric signal identification,
8) atmospheric moments calculation, and
9) averaging.

The original signal processing resident on the NASA 50-MHz profiler consisted of the same steps. To produce better quality and higher temporal resolution wind profiles for potential launch support, MSFC incorporated the wind's time and height continuity into the MFFG algorithm for use on the NASA/KSC 50-MHz profiler (Wilfong et al. 1993). The MFFG algorithm is limited to the signal identification and moments calculation portions of the profiler signal processing. The time domain averaging, conversion to the frequency domain, and the spectral averaging are all performed on a real-time processor that does not provide access to intermediate results from any of the signal-processing steps. The MFFG algorithm is a three-step process. First, the averaged spectra are filtered over time to reject spurious echoes, then the wind signal is identified within the power spectrum, and finally, the wind's velocity and other characteristics are computed. The MFFG algorithm produced near-real-time profiles and has been used to support vehicle launches since 1994.

The MFFG algorithm begins by applying a running temporal median filter (usually a three-point filter) to successive spectra from the oblique beams. Median filtering has the advantage of being able to filter transient interference and yet does not smooth over real atmospheric change as averaging does. Since velocity estimates are computed for every cycle (the power spectrum used to compute velocity estimates for time $t0$ is that produced by taking the three-point median filter of the spectra from $t0$, $t - 1$, and $t - 2$.), the median filter delays the detection of an atmospheric change for two cycles at worst. The temporal median filter is not applied to the vertical beam because in Florida the vertical velocities are minute and highly variable. Also, it is generally desirable to observe short timescale variations, those on the order of the radar cycle time or less, in the vertical velocities. Instead of a temporal median filter, the MFFG algorithm applies a five-point running mean

to smooth the single-cycle power spectrum, making the wind signal easier to identify.

Although the capability of applying the vertical velocity correction is available, it is generally not applied. The terrain in this part of Florida is very flat, and the vertical velocities are usually negligible. Because of its variability and low magnitude relative to the horizontal velocities, the vertical velocity is primarily used as a data quality indicator. In a sample of nearly two million vertical velocity estimates from the KSC profiler, the mean was 0.0016 m s^{-1} with a standard deviation of 0.37 m s^{-1}. The probability of the vertical velocity exceeding ± 1 m s^{-1} is 0.004. Applying the vertical velocity correction under these conditions would introduce as many errors as it had the potential to correct. Strong vertical velocities are usually associated with convection in which case the homogeneity assumption is violated. Strong vertical velocities are used to signify probable nonrepresentative wind profiles. When the profiler is used to support launch operations, the end data users are alerted that the strong vertical velocities are indicative of the profiler wind estimates not being representative of the true horizontal wind field. Vertical velocity correction would necessarily have to be considered for locations where the vertical velocity component is larger.

Once the spectral estimates have been temporally filtered, the MFFG algorithm computes the noise, interpolates over the zero Doppler shift, and then identifies the wind signal from within the power spectrum. As in most profilers, the noise is computed by applying the method of Hildebrand and Sekhon (1974). The MFFG applies a three-point log interpolation over the zero Doppler shift signal in order to reduce the effects of ground clutter. This works well in most cases since in the oblique beams the atmospheric signal is usually distinct from the ground clutter. When the atmospheric signal is not distinct from the ground clutter signal, the first-guess velocity and integration windows described below inhibit much of the bias imposed by the ground clutter. May and Strauch (1998) have quantified the potential biases due to ground clutter and recommend time-domain processing coupled with a three-point suppression to mitigate the effects of the ground clutter. Due to hardware implementation of the original signal processing, modifications to the signal processing, such as the MFFG algorithm, are limited to the averaged spectra. Eventual modernization of the 50-MHz profiler will make time-domain signal-processing improvements possible.

The wind signal within the frequency spectrum is identified by applying the wind's time continuity to the signal selection process. First, a first-guess radial velocity is chosen for each range gate within each beam. In general, the antecedent radial velocity is chosen (see later section for selecting the first-guess velocity for initialization and error recovery situations.). This velocity is converted to its frequency shift equivalent and
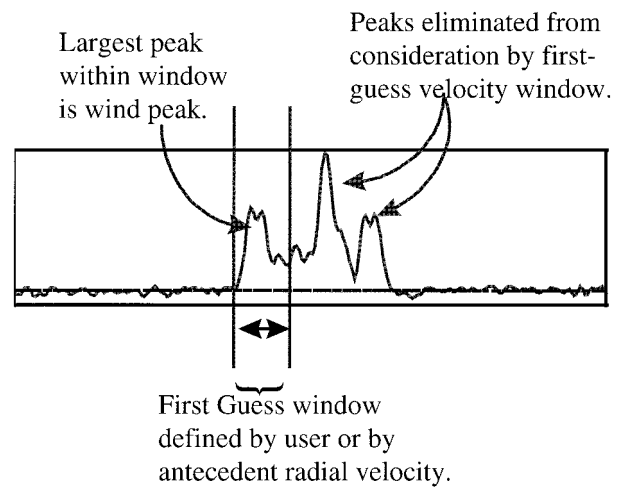

FIG. 1. Effect of first-guess velocity constraining window.

then a window about this frequency shift is defined in the power spectrum, as shown in Fig. 1. The MFFG algorithm constrains its search for the wind signal to this window, thus eliminating persistent interference signals from affecting the wind computations. The peak associated with the maximum spectral value within the first-guess window is selected as the wind signal. Based upon our early algorithm evaluation, the first-guess window is normally set to 12 frequency bins or about ± 1.5 m s^{-1}. This window can be narrowed to exclude any interference signal from consideration in the atmospheric signal identification portion of the algorithm.

Once the wind signal is identified, the radial velocity is computed at each range gate. In NOAA profiler wind calculation algorithms, the integral of the spectral power density minus the noise is taken from the maximum signal point within the identified wind peak down to the noise level (on both sides of the peak signal) and defined as the signal power. To minimize contamination from overlapping interference signals, we constrain this integral with a combination of two techniques: 1) a maximum integration window and 2) a maximum differential between the signal peak and the lowest signal (above the noise level) included in the integration. The MFFG algorithm uses the most restrictive window in defining the signal power to avoid situations in which the spectrum does not drop below the noise level between adjacent wind and interference peaks. Figure 2 illustrates the effects of the integration window and maximum difference limit. The integration window and associated difference limit considerably reduce the effects of the interference signal, although they do not eliminate its effects completely as is evident in Fig. 2. Further work is necessary to determine a better method to eliminate the effect of overlapping interference peaks.

The signal power is defined to be the area under the curve minus the noise bounded by the final determination of the integration window. The average Doppler shift is then computed by taking a weighted average of
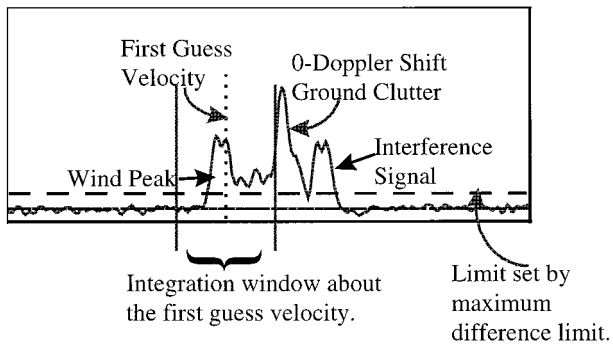
FIG. 2. Effect of integration constraining techniques.

the frequency bins within the integration window. The signal strength at each frequency bin is the weight applied during the averaging. The average Doppler shift is then converted to a radial velocity using the following relationship:

$$V_r = \frac{f_D \lambda}{2}, \tag{1}$$

where V_r is the radial velocity along the beam, f_D is the frequency Doppler shift, and λ is the wavelength.

MFFG algorithm has built into it two automated quality-control components. First, if the signal-to-noise ratio is below -15 dB for a given range gate, then the "measured" radial velocity for that range gate is replaced by the radial velocity component of the first-guess velocity. This is necessary because the MFFG algorithm (as well as the signal detection algorithms used on the NOAA profiler) will find an atmospheric signal whether or not one is evident above the noise level (May and Strauch 1989). The first-guess velocity and associated window for subsequent cycles remain the same. If the first-guess velocity for a given oblique beam is propagated more than four times successively for a given range gate then the radial velocity components from both oblique beams are replaced by an average of the radial velocities obtained by smoothing the vertical profile with a five-point running mean about the gate in question. In this case, the first-guess velocity is replaced by the resulting smoothed value. The number of times either the first guess is propagated or the resulting velocity is replaced by the average of the surrounding velocities is reported in the data output stream.

The second quality-control feature incorporates the wind's height continuity. The wind shear allowed between two range gates is limited by a critical shear value and a critical shear differential. The vertical shear ΔV at range gate k is defined by

$$\Delta V_k = V_k - V_{k-1}, \tag{2}$$

where V_k is the equivalent horizontal velocity in an oblique beam at the kth range gate. If the absolute value of ΔV exceeds 7 m s^{-1} gate^{-1} based on the expected mean extreme shears determined by Reiter (1969), at

gates k and $k + 1$, and the absolute value of the difference between the vertical shears at gates k and $k + 1$ is greater than 14 m s^{-1} gate^{-1} then the velocity calculated at gate k is deemed incorrect and is replaced by the average of the velocities at gates $k + 1$ and $k - 1$. The automated shear quality control works well for individual outliers, but it is susceptible to a height-continuous group of bad data points. If the wind estimates are being monitored, it is possible to force the algorithm to ignore the bad values by manually adjusting the first-guess velocity at each of the affected range gates.

a. Formulation of the first-guess velocity

The first-guess velocity and its associated window are powerful tools for reducing the probability of selecting an interference return in lieu of the atmospheric signal; however, the first-guess velocity must be chosen with care. Our approach to the first-guess formulation is to use "prior knowledge" of the wind profile coupled with interactive quality control. In general, the first-guess velocity for a given radar cycle is the velocity measured the previous cycle. Selection of the first-guess velocity at algorithm initialization is slightly more difficult. When available, initialization with a local rawinsonde is possible. Otherwise, the algorithm allows for the expansion of the first-guess window to include the entire spectrum. In this case, the strongest signal within the spectrum will be selected as the first-guess velocity, provided the shear control criteria are met. The resulting radial velocity profile can then be examined manually and the first-guess velocity adjusted at range gates where the algorithm has locked onto the incorrect signal. The latter case is evident when comparing a beam's radial velocity profile to contours of the spectral power density.

b. Manual quality control

The MFFG algorithm works well the vast majority of time, eliminating interference signals from consideration in the radial velocity calculation. At times, however, persistent interference close to the wind signal in the frequency spectrum can mask the signal because it is not practical to narrow the first-guess and integration windows to exclude the interference signal(s). In such cases, the resulting radial velocity may be contaminated by the interference. For upper-level wind evaluation prior to a vehicle launch or shuttle landing, however, contamination-free wind profiles are essential. To accommodate the specialized needs of the launch community, it is necessary to quality control radial velocities before they are combined into horizontal velocities and released to the data users.

Quality control of the radial velocity profiles consists of examining the power spectrum for each range gate and comparing it to the radial velocity computed for that gate. Profiles that contain data contaminated by
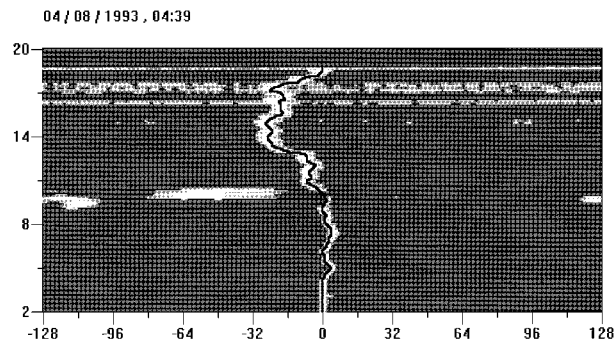
04 / 08 / 1993 , 04:39

FIG. 3. Example of interactive quality control display from the southeast beam (135°) at 0438 UTC 8 April 1993.
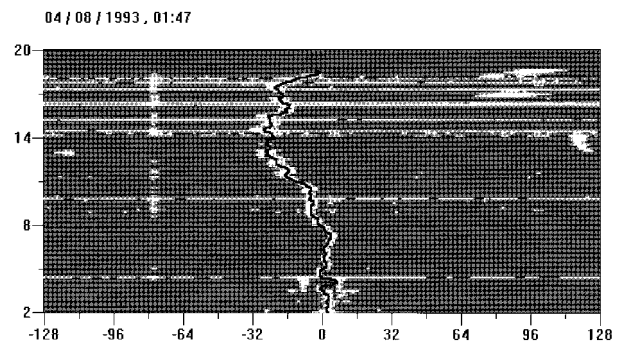

04 / 08 / 1993 , 01:47

FIG. 4. Example of interactive quality control display from the northeast beam (45°) at 0147 UTC 8 April 1995.

interference signals are rejected and not released to the data users. Figure 3 is an example of the interactive display used to quality control the data in real time. All 112 range gates are visible at once. The averaged spectra are color coded based upon signal strength and plotted in the background. The darker colors correspond to weaker signals and the brighter color corresponds to stronger signals. The signal is normalized within each range gate so that weaker signals at higher levels are not masked by the stronger signals at the lower range gates. The black line is the radial velocity trace through all the range gates, as computed by the MFFG algorithm.

Several very strong interference signals are visible in Fig. 3, and it is evident that the first-guess window excludes them from the radial velocity calculation. The brighter lines near the top of the profile (16.5–18.5 km) correspond to range gates where the signal is very weak. Figure 4 is an example of a case where interactive quality control is necessary. In this case, the algorithm has selected an apparent sidelobe signal as the wind signal rather than the ''true'' wind signal at about 4-km altitude. This profile must be rejected and the first-guess velocity must be modified in order to correct subsequent

profiles. In general, it takes 2–3 radar cycles to ensure that modifications to the first-guess velocity and first-guess and integration window sizes are sufficient to correct the algorithm.

c. Operational configuration

The MFFG algorithm is intended to run unattended with occasional monitoring for quality. Adjustments to the algorithm's parameters can be made whenever necessary. During launch countdowns, the MFFG algorithm profiles are continuously quality controlled prior to their release to the data users to ensure that the wind estimates are as representative as possible. Modifiable algorithm parameters and their default values are listed in Table 1.

The implementation of the MFFG algorithm allows the user to modify any of the available parameters. In practice, however, the only ones modified are the first-guess and integration windows and the first-guess velocity. The MFFG algorithm generates its own first-guess velocity, and it is necessary to modify it only when an interference signal is being tracked rather than the wind. The constraining windows effectively elimi-

TABLE 1. Operational configuration of MFFG algorithm parameters.

Parameter	Default	Description and effect
First-guess velocity window width	12	Constrains the search for the first velocity to six Doppler frequency bins either side of the first-guess velocity. The default is approximately equivalent to ± 1.5 m s^{-1}.
First-guess velocity	Previous radial velocity	Center of first-guess velocity window.
Integration window	20	Constrains the interval over which the signal power is calculated to 10 Doppler frequency bins either side of the maximum spectral power density. This is approximately equivalent to ± 2.5 m s^{-1}.
Cut-off percent	0.01	Percent difference between the maximum spectral power density and the spectral power density of the frequency bins included in the signal power integration. In this case, the integration window limits occur when the spectral power density drops 1% from its maximum value.
Number of points in temporal median filter	3	Number of radar cycles included in the temporal filter applied to the oblique beams' spectra.
Number of points in vertical beam smooth	5	Number of points included in the running average that smooths the vertical beam's spectra.
Vertical velocity correction	Off	Determines whether or not the vertical velocity correction is applied.

nate interference signals without masking genuine shears. The first-guess and integration window are applied independently and allow for real temporal wind changes of up to one-half the sum of the first-guess and integration windows or approximately 4 m s^{-1} over a 5-min window.

4. Performance

The performance evaluation of the DRWP using the MFFG algorithm was evaluated four different ways. Prior to its real-time implementation on the operational DRWP system, we compared the profiles produced by the DRWP using the MFFG algorithm to those measured by radar-tracked jimspheres in order to provide an understanding of the relative performance of the two systems. Comparisons of MFFG algorithm and 30-min consensus-averaged profiles are also presented to illustrate the differences between the two wind estimation methods and to demonstrate the importance of higher-temporal resolution profiles.

We also examined the general quality of the DRWP MFFG algorithm wind profiles over an extended amount of time. The wind estimates produced by the 50-MHz DRWP using the MFFG algorithm over a 6-month period were subjected to intense postanalysis quality control. The data were collected in support of a midtropospheric wind change climatology. The quality control rejected only a small fraction of the total number of wind estimates, indicating that the MFFG algorithm is robust and capable of producing highly reliable wind profiles.

Finally, we evaluated the performance of the 50-MHz DRWP using the MFFG algorithm on a case in which there was a known strong temporal wind shear. This case study highlights the value of high-temporal resolution wind profiles now available from the 50-MHz profiler using the MFFG algorithm (Schumann et al. 1995).

a. Comparison of MFFG DRWP wind profiles to time-proximate jimsphere and DRWP consensus wind profiles

Since the jimsphere is the current accepted standard for wind measurements at KSC/Cape Canaveral Air Station (CCAS), it is important to have a thorough understanding of the relative performance and advantages and disadvantages of the jimsphere and DRWP systems. Consequently, a comparison of jimsphere and DRWP profiles was performed. Although this analysis does not provide an absolute measure of the quality of the data from the DRWP, it does provide a relative measure of performance of the DRWP and information regarding the advantages and disadvantages of the DRWP.

The performance of the radar-tracked jimsphere (a radar-reflective balloon) and associated data reduction software has been studied by several authors, most re-

cently by Wilfong et al. (1997). The jimspheres are released from the CCAS weather station located approximately 15 km southeast of the profiler site. The jimsphere rises at a rate of about 5 m s^{-1} (varies slightly with altitude) up to about 16 km where it begins to drift rather than continue to rise. For the following comparisons and analyses, the jimsphere wind profile component velocities were converted to component velocities along the profiler's oblique beam's azimuths. After this conversion, the jimsphere component velocities (reported at 30.5-m intervals) were interpolated to the 50-MHz profiler reporting altitudes (at 150-m intervals).

In addition to the jimsphere versus MFFG wind profile comparisons, the wind profiles produced by the MFFG algorithm were compared to time-proximate consensus-averaged DRWP wind profiles. At the time these samples were taken, the cycle time of the radar was 3 min, resulting in 10 single-cycle estimates every half hour. This analysis provides a quantitative measure of the differences in performance between the two methods of profile estimation and the advantages and disadvantages of the two methods.

Since the mean winter and summer tropospheric wind profiles over the Florida peninsula are considerably different, this analysis evaluates the relative performance of the MFFG algorithm in both regimes. The analyses of the summer and winter regimes are based on jimsphere and profiler data from 12 September 1991 and 23 January 1992, respectively. The 12 September 1991 dataset contains profiles from five jimspheres released over a 5-h period; and the 23 January 1992 dataset consists of profiles from three jimspheres released over a 4-h period. For both of these datasets, we have computed and examined the root-mean-square (rms) differences of the northeast and southeast velocity components between time proximate jimsphere and MFFG wind profiles and between time-proximate consensus-averaged and MFFG wind profiles.

Similar comparisons between DRWP consensus-averaged profiles and balloons have yielded differences in the u and v components between 1.5 and 5.0 m s^{-1} (May 1993; Weber and Wuertz 1990), depending upon the height of the measurements and the effective SNR. The difference between the comparisons presented here and others is that the MFFG profiles are not averaged over the time it takes the balloon to rise. Instead, we used an MFFG profile taken shortly after the release of the jimsphere to evaluate the difference between looking at high-temporal resolution profiles measured nearly directly overhead and looking at point measurements in time along a slanted path defined by the wind field itself.

Likewise, the MFFG profiles were not averaged in their comparison to the consensus-averaged profiles. Instead, the comparisons highlight the differences between looking at high-temporal resolution data and consensus-averaged data. The original system did not accommodate quality control of the consensus-averaged profiles and thus no quality control was applied to the consensus-

TABLE 2. Jimsphere and MFFG algorithm DRWP velocity comparisons for 12 September 1991.

Jimsphere profile time (UTC)	MFFG algorithm profile time (UTC)	rms differences southeast beam (m s^{-1})	rms differences northeast beam (m s^{-1})
1842	1912	1.47	1.56
2009	2038	1.79	1.56
2057	2128	1.42	1.54
2147	2217	1.78	1.89
2326	2358	1.60	1.39

TABLE 4. Consensus-averaged and MFFG wind algorithm DRWP velocity comparisons for 12 September 1991.

Consensus profile time (UTC)	MFFG algorithm profile time (UTC)	rms differences southeast beam (m s^{-1})	rms differences northeast beam (m s^{-1})
1900	1915	0.79	0.57
1930	1946	0.87	0.71
2000	2015	0.87	0.71
2030	2044	0.80	0.80
2100	2116	0.70	0.63
2130	2145	0.72	0.85
2200	2214	0.76	0.76
2230	2246	0.72	0.59
2300	2314	0.91	0.81
2330	2346	0.51	0.40

averaged profiles. The MFFG profiles were generated assuming a reasonable first-guess velocity with no further quality control. Note that unless there is significant interference within the first-guess and/or the integration windows, a reasonable first guess ensures that the resulting wind estimate is not contaminated by interference.

The rms differences between the MFFG algorithm and the jimsphere profiles from 12 September 1991 and 23 January 1992 are shown in Tables 2 and 3, respectively. The rms velocity difference between two jimspheres separated by 50 min on 12 September 1991 is 1.7 m s^{-1}, which is very similar to the magnitude of the rms velocity differences between the MFFG algorithm profiles and the jimsphere profiles from the same day. The temporal separation between the two 23 January 1992 jimspheres was too large to use as an rms reference measure, so we examined the rms differences between two MFFG algorithm profiles. The rms velocity differences between two MFFG algorithm profiles separated by 30 min on 23 January 1992 are approximately 2.2 m s^{-1}. This is consistent with the relatively larger rms differences between the MFFG algorithm and jimsphere profiles listed in Table 3. Tables 4 and 5 contain the rms velocity differences between the consensus-averaged profiles and the MFFG algorithm profiles from the approximate midpoint of the consensus interval for the same two days. The rms differences between the consensus-averaged and MFFG algorithm profiles are considerably less than the differences between the MFFG algorithm and jimsphere profiles. This probably reflects the difference in spatial variability. The consensus-averaged and MFFG algorithm profiles both sample the air space directly overhead. On the other hand, the jimspheres are released approximate 15 km southeast of the profiler site and travel downwind as they rise.

Composite rms differences were computed for MFFG algorithm and consensus-averaged wind estimates (Table 6). The sample consisted of 10 profile comparisons from 12 September 1991, 10 profile comparisons from 23 January 1992, and 12 profile comparisons from 20 February 1992. Each profile contains a radial velocity estimate for 112 range gates spaced at 150 m for a potential of 3584 observations. In this case, the consensus averaging method failed to reach a consensus for 73 of the observations for a total sample size of 3511. The MFFG algorithm profile from the center of the consensus-averaging period was used to compute the differences. The distribution of the vector differences is plotted in Fig. 5.

Figures 6–9 contain representative northeast and southeast profiles of horizontal wind velocity components as measured by the jimsphere and the profiler using both the MFFG and consensus-averaging methods. As would be expected in a time-continuous wind field, most of the large-scale features present in all of the profiles are very similar. Some differences in the small-scale features, however, illustrate the effect of the different sampling methods. For instance, the consensus-averaging method failed to detect temporal changes between 6 and 8 km and between 8 and 11 km on the

TABLE 3. Jimsphere and MFFG wind algorithm DRWP velocity comparisons for 23 January 1992.

Jimsphere profile time (UTC)	MFFG algorithm profile time (UTC)	rms differences southeast beam (m s^{-1})	rms differences northeast beam (m s^{-1})
1400	1408	1.90	1.52
1530	1530	2.06	1.76
1730	1729	2.21	1.93

TABLE 5. Consensus-averaged and MFFG wind algorithm DRWP velocity comparisons for 23 January 1992.

Consensus profile time (UTC)	MFFG algorithm profile time (UTC)	rms differences southeast beam (m s^{-1})	rms differences northeast beam (m s^{-1})
1300	1314	0.80	0.60
1330	1343	0.96	0.81
1400	1416	0.98	0.84
1430	1445	0.91	0.64
1500	1518	0.93	0.77
1530	1546	0.73	0.93
1600	1615	1.04	0.91
1630	1652	1.18	1.12
1700	1717	1.07	0.75
1730	1746	1.03	0.92
1800	1815	1.85	1.65
1830	1843	1.70	1.10

TABLE 6. The rms difference between consensus-averaged and MFFG algorithm wind estimates based upon 3511 samples.

	Southeast beam (m s⁻¹)	Northeast beam (m s⁻¹)	Vector difference (m s⁻¹)
rms difference	0.88	0.79	1.18

FIG. 5. Distribution of vector differences between MFFG algorithm and consensus-averaged wind estimates from 3511 samples.

23 January 1992 profile (Figs. 8 and 9). Examination of a series of MFFG algorithm profiles from 1314 to 1509 UTC indicates 1) decreases in the southeast beam velocities as large as 8 m s⁻¹ between 6 and 8 km, 2) increases in the northeast beam velocities as large as 10 m s⁻¹ near 8.5 km, and 3) increases as large as 2–3 m s⁻¹ between 9 and 11 km.

Other noticeable differences between profiles are the erroneous wind estimates near 13 and 16 km on the 23 January 1992 consensus-averaged profile due to the invalid assumption that the maximum special power density is associated with the atmospheric signal. The large-scale features present in the DRWP and jimsphere profiles are very similar; however, the small-scale features exhibit differences, particularly in the southeast beam velocities. The differences in the small-scale features are not surprising in light of the spatial and temporal differences in data collection between the jimsphere and the DRWP.

Figures 10 and 11 illustrate the distribution over height of the rms differences between consensus average and MFFG algorithm profiles and between jimsphere and MFFG algorithm profiles. As would be expected the rms differences between the consensus average method and the MFFG algorithm are considerably smaller than the rms differences between the jimsphere and the DRWP using the MFFG algorithm. For the jimsphere versus MFFG differences, the rms values rise steadily as the altitude increases especially in the winter where the jet stream causes further separation between the profiler and the jimsphere. The relatively large rms differences between the consensus-averaging method and the MFFG algorithm from about 5 and 10 km are likely due to interference signals contaminating the consensus average. Persistent interference is often evident at these altitudes. Thirteen kilometers is generally high for persistent interference to contaminate the spectrum, thus the peak in the rms differences between the consensus-averaging method and the MFFG algorithm in the northeast beam at this altitude is likely due to lack of signal rather than interference.

In addition to the horizontal velocity comparisons, we have computed the coherence between the northeast and southeast velocity components between two time-proximate jimsphere and MFFG wind profile pairs to determine the linear correlation between the profiles. The degree of correlation between the jimsphere profiles and the MFFG wind algorithm DRWP profiles was quantified by cross-spectrum analysis. One of the products of cross-spectrum analysis is the coherency spec-
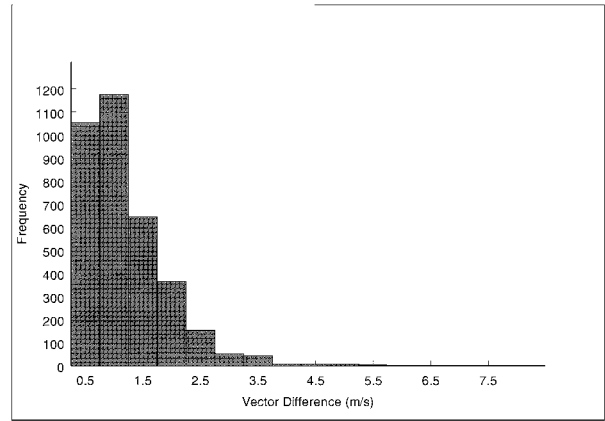
trum, which measures the correlation between the two signals (e.g., profiles) at each wavelength (Jenkins and Watts 1968). The square of the coherency can vary between 0 and 1 and is analogous to the square of the correlation coefficient, except the coherency is a function of wavelength. As the square of the coherency ap-
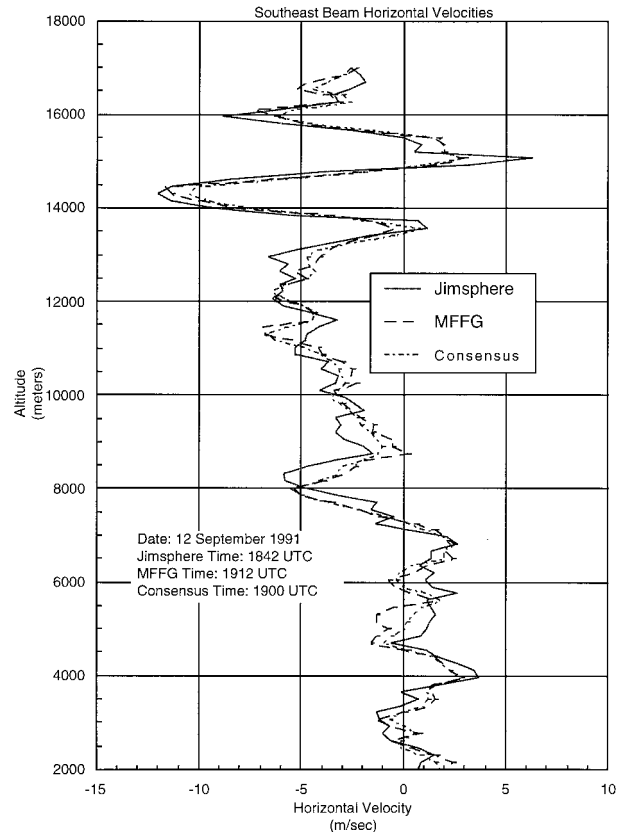

FIG. 6. Southeast beam velocities for 12 September 1991. Profile time stamps are jimsphere 1842 UTC, consensus 1900 UTC, and MFFG wind algorithm 1912 UTC.
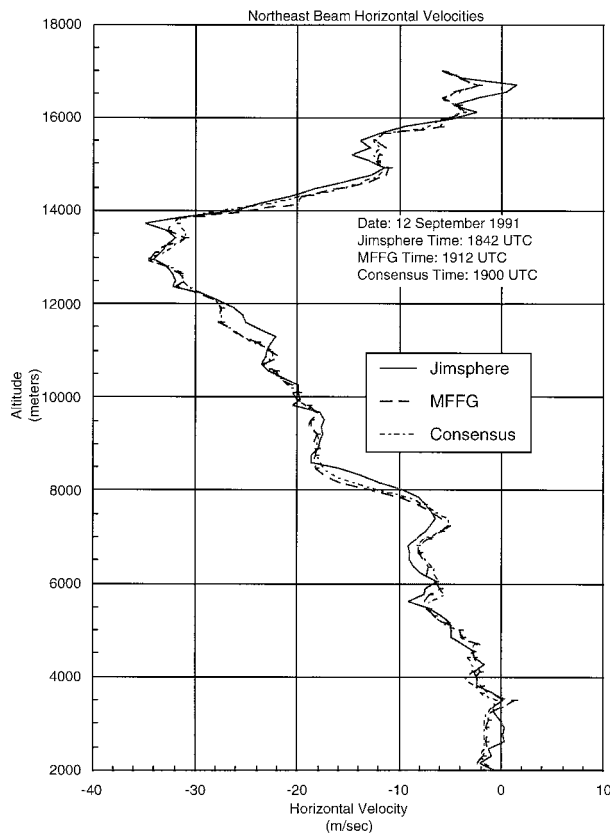
FIG. 7. Northeast beam velocities for 12 September 1991. Profile time stamps are jimsphere 1842 UTC, consensus 1900 UTC, and MFFG wind algorithm 1912 UTC.
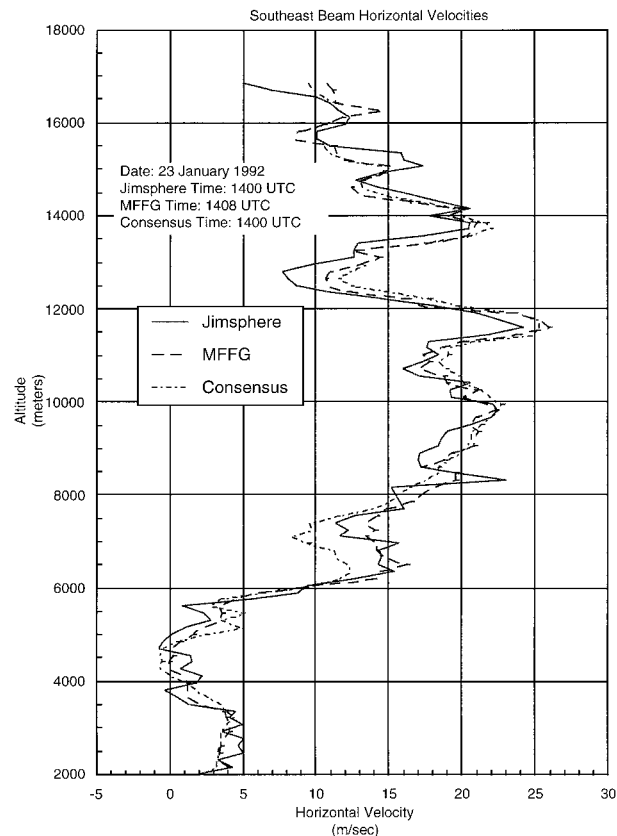
FIG. 8. Southeast beam velocities for 23 January 1992. Profile time stamps are jimsphere 1400 UTC, consensus 1400 UTC, and MFFG wind algorithm 1408 UTC.

proaches 1 for a given wavelength, then the two signals are highly linearly correlated at the given wavelength. Conversely, as the square of the coherency approaches 0 for a given wavelength, then the two signals are not linearly correlated at the given wavelength.

Figures 12 and 13 illustrate the coherency analysis performed on the 12 September 1991 and 23 January 1992 jimsphere and MFFG algorithm DRWP profiles. The data in Fig. 12 indicate both components of the 12 September 1991 jimsphere and MFFG wind algorithm DRWP profiles are highly coherent (i.e., coherency squared values of ~0.7 or greater) to wavelengths as short as 1400 m (i.e., wave number 4.5×10^{-3} m^{-1} where wavenumber equals 2π/wavelength). At shorter wavelengths, the coherence of the northeast beam velocities remains relatively high, whereas the coherence of the southeast beam velocities is generally less. This is expected since the small-scale features exhibited greater differences in the southeast beam velocities than the northeast beam velocities (Figs. 6 and 7). The coherence data in Fig. 13 indicate both components of the 23 January 1992 profile are highly coherent to wavelengths as short as 1100 m (i.e., wavenumber 6×10^{-3} m^{-1}).

In addition to the velocity comparisons between the

MFFG algorithm DRWP profiles and the consensus-averaged DRWP profiles, the number of levels where the velocity extraction techniques are either unable to produce a velocity estimate or produce an erroneous velocity have been catalogued and analyzed. These data are important in evaluating the relative performance of the two techniques and are also an important measure of the data quality.

Table 7 contains the number of levels where the consensus averaging technique was unable to produce a velocity estimate or produced an erroneous velocity (i.e., a velocity estimate that is clearly unrealistic) for the data from 12 September 1991. The table also contains the number of levels where the first-guess velocity has been propagated more than two times consecutively by the MFFG algorithm. The critical value for the number of first-guess propagations has been selected in relation to the proposed use of the DRWP in support of shuttle operations. At this time, proposed use of the DRWP calls for a wind profile to be distributed to the customer at least every 15 min. With a cycle time of 5 min, this means every third wind profile would be transmitted to the customer. Therefore, if the first-guess velocity is propagated three or more times consecutively, the customer is not provided with a new estimate of the
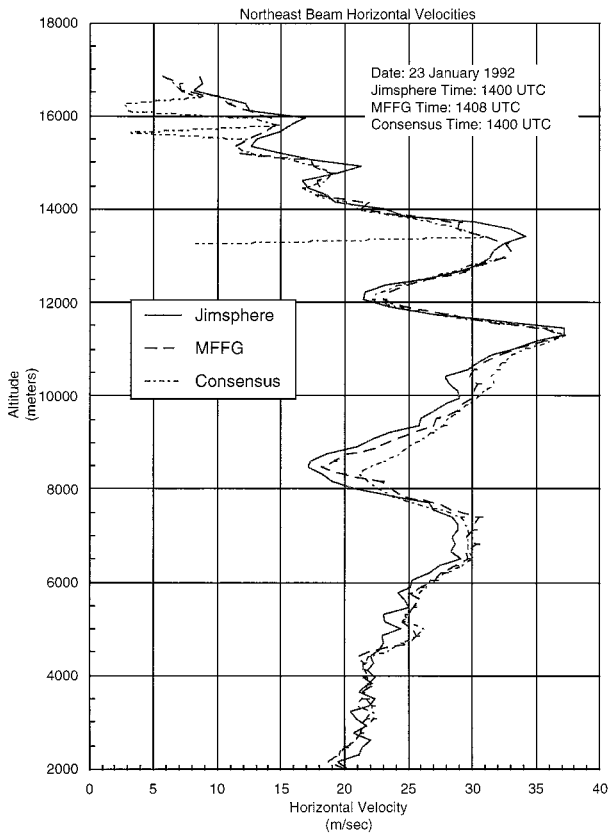
FIG. 9. Northeast beam velocities for 23 January 1992. Profile time stamps are jimsphere 1400 UTC, consensus 1400 UTC, and MFFG wind algorithm 1408 UTC.

wind at that particular level. Hence, the critical value for the number of first-guess propagations was set at two.

The data in Table 7 indicate both velocity extraction techniques were able to produce reasonable velocity estimates at most levels throughout the 5-h period on 12 September 1991. The number of levels where the first-guess velocity was propagated more than two times consecutively by the MFFG algorithm is slightly higher than the number of levels reporting missing or erroneous data by the consensus technique. The MFFG algorithm propagates the first-guess velocity whenever the SNR is below −15 dB. The fact that the first-guess velocity was propagated does not indicate that the MFFG algorithm could not find a solution, only that the SNR of the measured velocity was below the allowable minimum.

The results from 23 January 1992 data (Table 8) are indicative of the drier conditions in the region during the winter months, resulting in lower SNRs above 13 km. Consequently, the number of levels where the consensus-averaging technique was unable to produce a velocity estimate or produced an erroneous velocity and the number of levels where the first-guess velocity has been propagated more than two times consecutively by
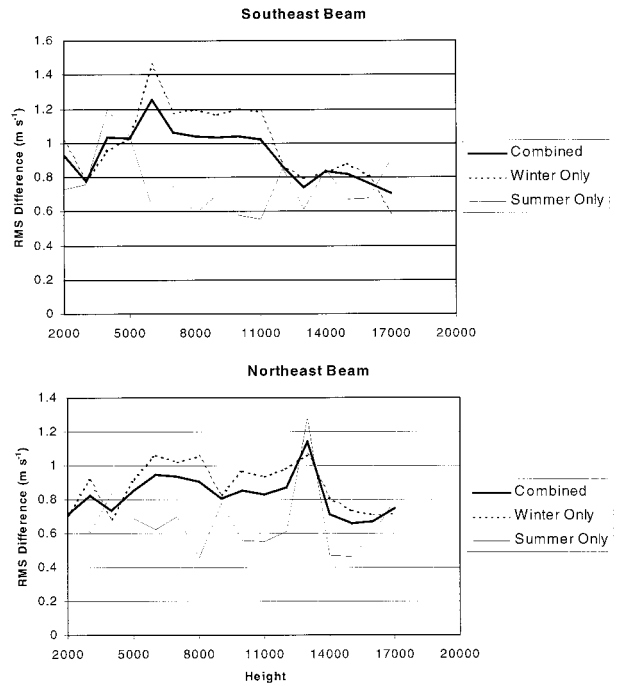

FIG. 10. Height distribution of rms differences between consensus average and MFFG algorithm profiles.

the MFFG algorithm is greater for the 23 January 1992 data than for the 12 September 1991 data.

This case illustrates a significant operational difference between the two techniques. At 1800 UTC the
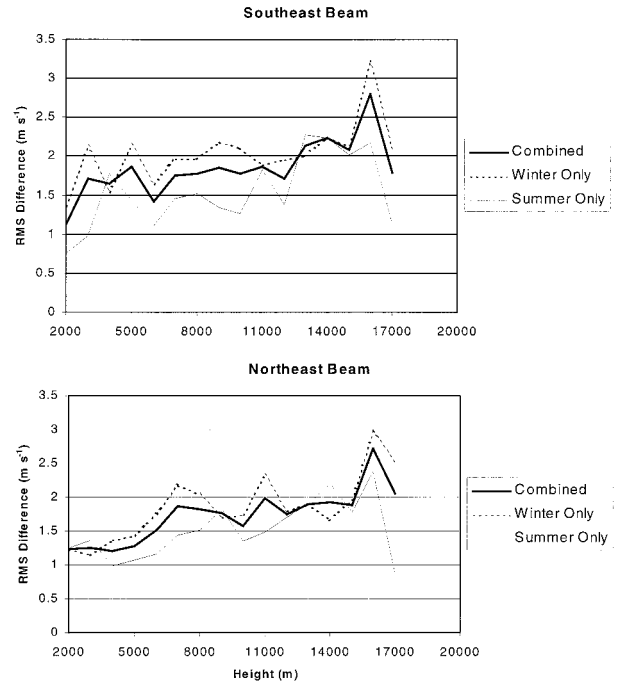

FIG. 11. Height distribution of rms differences between jimsphere and DRWP with MFFG algorithm profiles.

Date: 12 September 1991
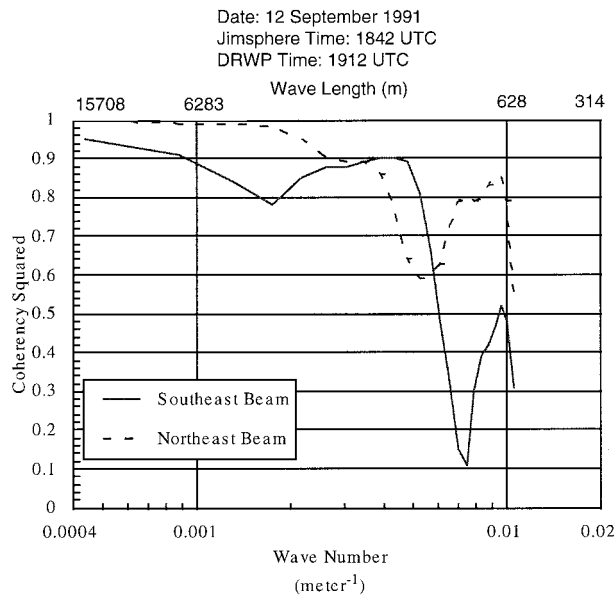Jimsphere Time: 1842 UTC
DRWP Time: 1912 UTC

FIG. 12. Coherency analysis of jimsphere and MFFG wind algorithm DRWP profiles for 12 September 1991. Profile times are jimsphere 1842 UTC and MFFG wind algorithm 1912 UTC.

TABLE 7. Consensus averaged and MFFG wind algorithm DRWP profile comparisons for 12 September 1991.

Consensus profiles		MFFG algorithm profiles	
Time (UTC)	Number of levels*	Time (UTC)	Number of levels**
1900	0	1915	0
1930	0	1946	1
2000	0	2015	1
2030	0	2044	1
2100	0	2116	1
2130	0	2145	2
2200	1	2214	0
2230	0	2246	1
2300	2	2314	1
2300	3	2346	3

* The number of levels with either erroneous data or missing data.
** The number of levels with the number of first-guess velocity propagations for the east beam and/or the north beam greater than two.

consensus-averaging procedure was unable to produce a velocity estimate or produced an erroneous velocity at 25 of the 112 levels. This is a result of the lightning contamination during the period from 1815 to 1830 UTC. Conversely, the first-guess velocity was propagated more than two times consecutively by the MFFG algorithm at only three levels on the 1815 UTC wind profile. Strictly speaking, this is not a truly fair comparison since the lightning contamination was from the period 1815 to 1830 UTC or just after the 1815 UTC MFFG algorithm profile. However, it does highlight an important difference between the two velocity extraction techniques. Poor signal returns for as brief a period as 15 min may result in a 1-h time span between two consecutive high-quality wind profiles from the consensus-averaging algorithm. In contrast, poor signal returns for a 15-min period would result in only a 20-min time span between two consecutive high-quality wind profiles from the MFFG algorithm.

Overall, the consensus-averaging technique was unable to form a consensus at a total of 94 levels over 31 different samples of 112 range gates each. The range gates where the consensus averaging was unable to form a consensus were all at 10 km or above, indicating that the primary culprit in the inability to form a consensus was lack of signal rather than interference. In general,

Date: 23 January 1992
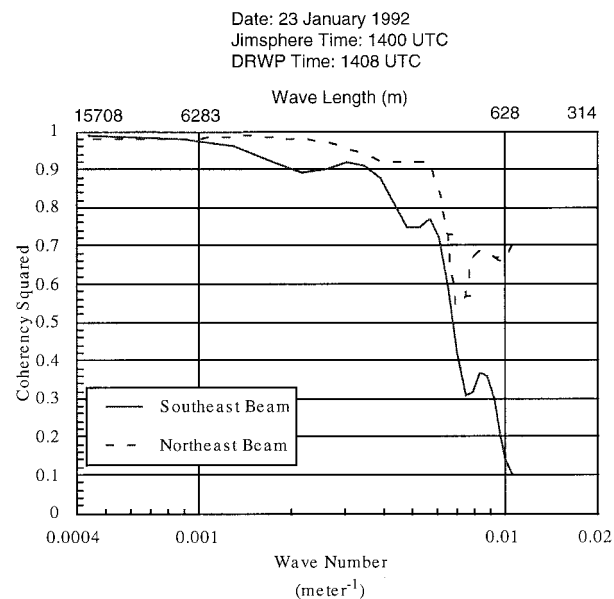Jimsphere Time: 1400 UTC
DRWP Time: 1408 UTC

FIG. 13. Coherency analysis of jimsphere and MFFG wind algorithm DRWP profiles for 23 January 1992. Profile times are jimsphere 1400 UTC and MFFG wind algorithm 1408 UTC.

TABLE 8. Consensus-averaged and MFFG wind algorithm DRWP profile comparisons for 23 January 1992.

Consensus profiles		MFFG algorithm profiles	
Time (UTC)	Number of levels*	Time (UTC)	Number of levels**
1330	0	1343	1
1400	5	1416	1
1430	3	1445	4
1500	2	1518	4
1530	5	1546	3
1600	7	1615	5
1630	0	1652	1
1700	2	1717	4
1730	1	1746	2
1800	25	1815	3
1830	1	1843	0

* The number of levels with either erroneous data or missing data.
** The number of levels with the number of first-guess velocity propagations for the east beam and/or the north beam greater than two.

interference is either filtered out by the consensus averaging or the interference affects enough of the single-cycle estimates to contaminate the consensus average.

b. Fraction of MFFG data accepted after rigorous quality control

Another indication of the performance of the MFFG algorithm is how well the data presented by the algorithm pass a rigorous quality-control process. In the course of conducting a midtropospheric wind change climatology, one of us had occasion to submit a large volume of wind estimates from the KSC 50-MHz profiler to intense quality control. A summary of the results is presented here, while the details are available in Merceret (1997).

Data were collected on 117 days between 29 September 1995 and 26 March 1996 during which the profiler was operational for all or a significant part of the day. Profiles of 112 gates each were taken every 5 min. Each range gate in each profile constitutes one record in the daily data files, resulting in 32 256 records per day. Each record contained a quality-control (QC) flag in which the individual bits indicated which test(s) the record had failed during the QC process. In some cases, one or more profiles were missing from a day's data. These records were filled with the value ''999'' for all variables and a ''missing data'' bit was set in the QC flag.

Four of the bits were reserved for QC indicators generated internally by the DRWP. These were set if threshold values for the following were exceeded: vertical speed, vertical shear, spectral width, and first-guess propagation. None of these flags was set during the entire experiment.

Four additional flags were set by an automated QC algorithm developed by Merceret (1997). These were triggered by excessive wind speed or direction shear, inadequate SNR, or failure to pass the small median test of Carr et al. (1995) with somewhat more stringent parameters. The small median test requires threshold values be designated for three different heights. Based upon 20 years of rawinsonde data, the thresholds used for this work were 5.7 m s^{-1} at 2 km, 10.2 m s^{-1} at 9 km, and 8.4 m s^{-1} at 16 km.

After the automated QC was run, each file was examined manually using a time–height visual display and information from operator's logs. Nearly all of the manual QC consisted of flagging the interior (in time–height space) of sidelobe and interference signatures whose boundaries were flagged by the automated process. In the interior of sidelobes, the gradients are small enough to pass the QC tests, but not on the edges.

The dataset of 117 days produced 3 773 952 records. Of these, 71 606 (19%) were flagged as missing data. There remained 3 057 936 records of actual data. Of the 117 days, 44 days (37.6%) required some manual flagging. Less than 1% of the data were manually flagged

TABLE 9. Records failing automated QC elements.

	Small median	Directional shear	Speed shear	Signal to noise
Number of records	7400	9953	2767	4495
Percentage	0.24	0.32	0.09	0.15

on these days with the largest amount on any one day being about 3.5%.

The automated QC algorithm caught nearly all of the sidelobes and interference signals, although it frequently only flagged their boundaries in time–height space. The small percentage of data flagged by the automated process as shown in Table 9 is an accurate indication that the DRWP data produced by the MFFG algorithm are generally clean. Less than one-third of 1% of the data were flagged.

The combined result of the postanalysis, automated, and manual QC process flagged less than one-half of 1% of the total sample of data.

c. Case study

Although the potential temporal resolution of the MFFG algorithm may be neither essential nor practical for many applications, the impact to the space launch community cannot be overstated (see for example Merceret 1998). Upper-air winds have a significant impact upon space vehicle launches at KSC and CCAS. The estimated stresses the launch vehicle will undergo (referred to as loads in the launch community) due to wind and the vehicle's flight path are computed several hours prior to launch using wind estimates from local rawinsonde and jimsphere balloon releases.

For historical and data-handling reasons, all vehicle loads are calculated using balloon-measured winds. The last loads calculation for shuttle, for example, is made approximately 35 min prior to liftoff and is made based upon a balloon released 2 h prior to a scheduled launch (i.e., $T - 120$ min). The rise rate of the balloons as well as data transfer and computation logistics prevent recomputing the loads using balloons released nearer to the scheduled launch time. In addition to the balloons released at and prior to $T - 120$ min, balloons are released at $T - 70$ min and at $T + 15$ min. The $T - 70$-min balloon is used to detect any significant wind changes occurring after the loads estimates are made, and the $T + 15$-min balloon is used to estimate the actual winds experienced by the shuttle. Other launch vehicles have their own balloon release schedules depending upon the vehicles' and their associated payloads' sensitivity to strong winds and wind shears.

Wind profiles generated by KSC's 50-MHz DRWP are monitored during the launch countdown to provide wind measurement redundancy and to detect any wind shifts occurring between balloons, especially those occurring after the last balloon prior to launch is released. Wind shifts occurring after the vehicle loads estimates

are calculated are scrutinized carefully, and, if necessary, the launch is held or scrubbed to ensure vehicle and, in the case of the shuttle, crew safety.

On 8 April 1993, a significant wind shift within a relatively shallow layer of the atmosphere occurred within the last hour prior to a scheduled shuttle launch. Liftoff ($T - 0$) for shuttle mission STS-56 was schedule for 0529 UTC on 8 April 1993. The jimsphere used for loads calculations was released at 0329 UTC, and the last jimsphere released prior to launch was released at 0419 UTC. Figure 14 contains the u and v component wind profiles measured by the $T - 120$ min (0329 UTC), $T - 70$ min (0419 UTC), and $T + 15$ min (0544 UTC) jimspheres. The differences between the $T - 120$ (the last profile used in the loads calculation) and the $T + 15$ profiles obvious in the 2-km layer from 11 to 13 km is only slightly evident in the profile measured by the $T - 70$-min balloon, indicating that most of the wind shift occurred during the last hour prior to launch. This shift amounted to a 25.3 m s^{-1} reduction in the expected tail wind on the shuttle that was used in the last load's estimation. Fortunately, this shift was detected by the profiler and the validity of the loads was evaluated prior to the actual launch, which occurred on time at 0529 UTC.

Figure 15 illustrates the difference between the jimsphere and MFFG algorithm wind profiles at $T - 70$ and $T + 15$ min. Figure 15 (a) contains the u and v component wind profiles as measured by the $T - 70$ min jimsphere overlaid with the time-coincident u and v component profiles measured by the 50-MHz DRWP; Fig. 15 (b) contains the u and v component wind profiles as measured by the $T + 15$-min jimsphere overlaid the time-coincident u and v component DRWP profiles. The differences between the profiler and jimsphere profiles, especially those evident between 11 and 13 km, are due to the time–space differences between jimspheres and wind profilers. Jimspheres rise at a rate of about 5 m s^{-1} and drift downwind as they rise.

First of all, the data presented in Fig. 15 provide reassurance that the wind shift detected by the jimsphere and profiler is real. This is an obvious benefit from having two independent instruments measuring critical winds. More importantly, however, Figs. 14 and 15 illustrate the significant advantage of having higher temporal resolution in the measurement of upper-level wind for space lift missions.

5. Conclusions and future direction

It has long been recognized that the signal processing resident on wind profilers must address the problem of multiple local maxima in the power density spectrum and that consensus averaging is not always successful at eliminating outliers. Further, it has been noted that the consensus-averaging method fails to detect rapidly changing wind fields and results in wind estimates that are nonrepresentative of the true atmospheric condi-
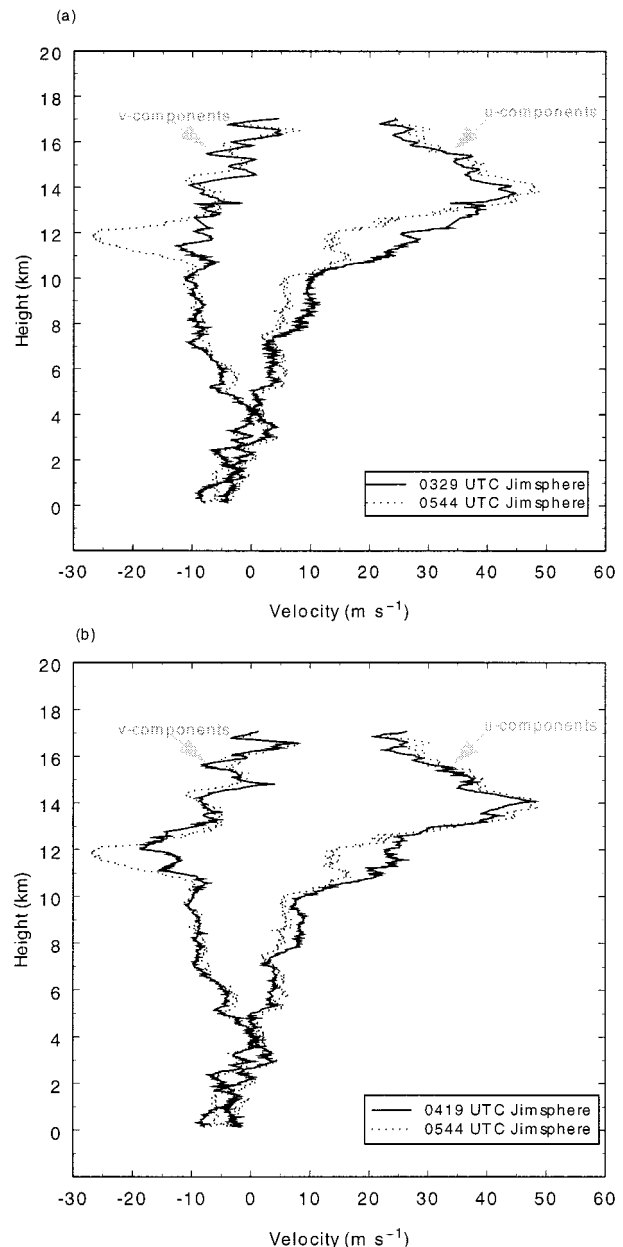

FIG. 14. Comparison of u and v wind velocity components at different times during 8 April 1993. (a) The wind profile at the time the last vehicle loads calculations were made to the wind profiles just after launch of STS-56. (b) The last balloon-measured wind profile prior to launch to the balloon-measured profile just after launch.

tions. Even block averaging will delay the detection of changing wind conditions.

Since their inception, the primary use of wind profilers has been for atmospheric research and synoptic wind field estimation, which thus far have been interested primarily in relatively long-term (half-hour or more) averages. Although synoptic atmospheric modeling may be unable to make use of the short-term fluctuations that can be identified using unaveraged profiler
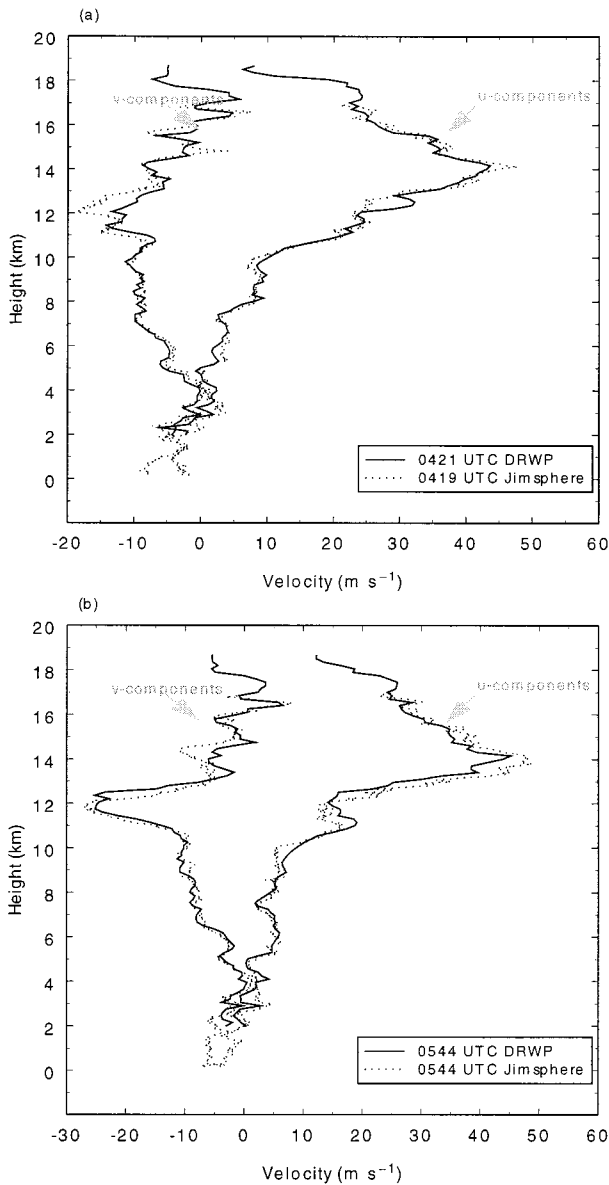
FIG. 15. Comparison of DRWP- and jimsphere-measured profiles. (a) The profiles measured 70 min prior to launch and (b) profiles measured 15 min after launch on 8 April 1993.

wind estimates, it is still important to eliminate contaminated data. This is best done at the single-cycle time frame—the results of which can still be averaged if that is desirable. Applications such as the vehicle launch programs require much higher-temporal resolution wind profiles than what have been available via either balloons or hourly profiler averages.

The 50-MHz profiler and the MFFG algorithm used to determine the wind velocities have attempted to provide contamination-free, high-resolution wind field estimates in near–real time since 1994. The analyses presented in this paper demonstrate that the use of profilers to provide real-time wind information is viable and po-

tentially crucial. Although care must be taken in the interpretation of high-temporal resolution wind estimates due to inhomogeneities in the atmosphere, it is possible and even beneficial to take advantage of the potential temporal resolution available from wind profiler's single-cycle wind estimates.

Analysis has shown that the KSC profiler using the MFFG algorithm is able to provide continuous, high-quality wind profiles indefinitely. Evaluation of how well the MFFG algorithm performs on profilers located elsewhere or operating at different frequencies has not been done. The improvements to the data quality available from the profiler due to the MFFG algorithm, however, have been substantial and have made it possible to consider making the profiler a primary source for upper-level wind measurements. The current research status of the profiler requires that an operational implementation of the profiler be evaluated. NASA is currently certifying the profiler for limited operational support and is investigating the cost–benefit ratio for upgrading the profiler to use five beams to identify the case of an inhomogeneous wind field. NASA is also continuing signal-processing research to eliminate the current need for manual quality control during critical operations.

APPENDIX

Hardware Description

The KSC 50-MHz Doppler Radar Wind Profiler has three major physical components: an antenna, a radar transceiver, and a data processing and control system. Each of these components will be discussed and their interconnection and interaction described in this appendix. This radar is an electrical and mechanical twin to
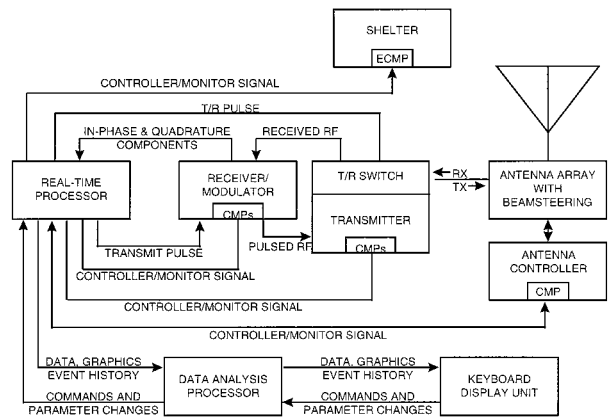

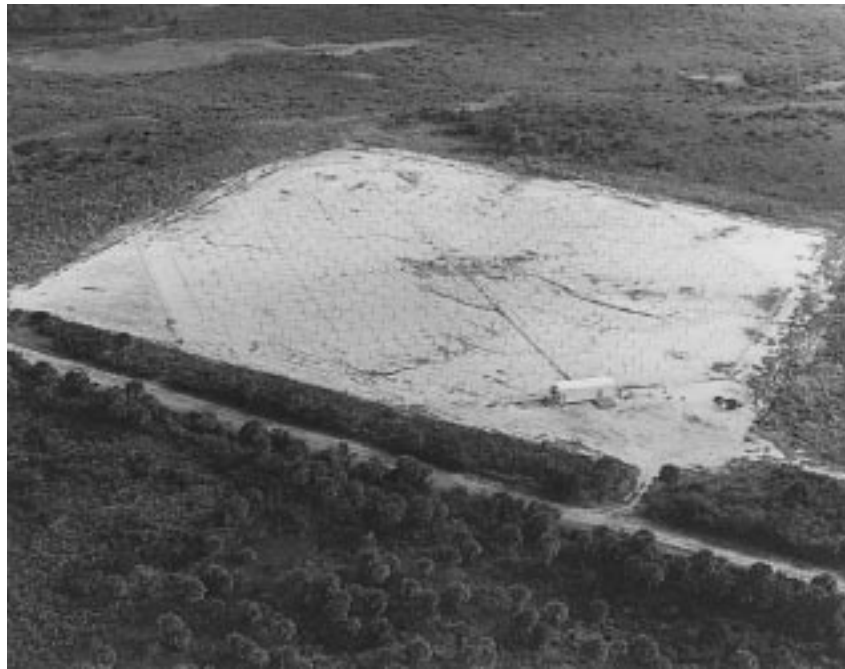FIG. A1. Functional block diagram of NASA KSC 50-MHz Doppler radar wind profiler.

FIG. A2. Aerial photograph of NASA KSC 50-MHz profiler. Coaxial–collinear phase array antenna along with shelter containing computer and hardware subsystems are visible.

the one described by Nastrom and Eaton (1995). It operates on a frequency of 49.25 MHz with a wavelength of 6.085 m. A functional block diagram is provided in Fig. A1.

a. Antenna

The DRWP antenna has a physical aperture of 15 600 m^2 and an effective aperture at 49.25 MHz of 13 500 m^2. It is located at 28°37′38″N, 80°41′45″W, adjacent

FIG. A3. NASA KSC 50-MHz DRWP antenna system functional block diagram.

to the Shuttle Landing Facility at Kennedy Space Center, Florida. A photograph of the profiler antenna and trailer housing the electronics is presented in Fig. A2. Beam formation is accomplished using a phased array of 168 coaxial–colinear (COCO) elements comprising two intermeshed sets of 84 elements at right angles. Its shape is an irregular octagon. The COCO elements are positioned about 1.5 m above a ground level electrical ground plane made of insulated stranded 14-gauge copper wire. The elements are attached to fiberglass catenaries suspended from wooden posts.

The array is driven by a system of coaxial phasing lines and power splitters, as shown in Fig. A3. The phasing is relay switched by the data processing and control system to sequentially produce three beams. One points straight upward and is called the vertical beam. The remaining two are inclined 15° from the vertical, one along an azimuth of 45° true, and the other along an azimuth of 135° true. The feedlines in the highest power portions of the array are made of 7.6-cm air-dielectric heliax cable. The cables directly supplying the COCO elements are 1.3-cm foam-dielectric heliax cable. The larger cables are pressurized to keep out moisture and contaminants. The beamwidth of each beam is 2.9°, and the average power aperture product of the antenna is 1.7×10^8 W m^2 at the rated peak power of 250 kW and a duty cycle of 5%.
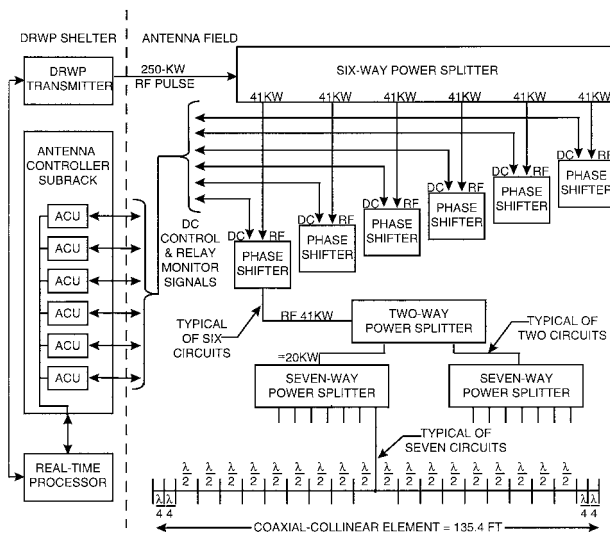
b. The transceiver

The radar transmits and receives pulses of radio frequency (RF) energy at a nominal frequency of 49.25

MHz, having a free space wavelength of 6.085 m. The pulse repetition frequency is 6250 s^{-1} corresponding to a pulse repetition period of 160 μs. Pulse coding is used to improve range resolution for a given pulse length. Each pulse is 8 μs long and consists of eight 1-μs phase modulated code elements. The same antenna and feedlines are used on transmit and receive. A transmit/receive (T/R) switch operated by the control system determines whether the antenna is connected to the transmitter or to the receiver.

The transmitter operates at 250-kW peak power with an approximate duty cycle of 5%. This power level is reached in three stages of amplification. A predriver raises the input pulse supplied by the Transmitter Control Unit (TCU) to 3.2 kW. A driver amplifier raises this to 26 kW and applies it to the final amplifier. Vacuum tubes are used throughout the high power stages. Standing wave ratios (SWRs) and critical voltages and currents are monitored continuously, and fault conditions will shut down the transmitter to prevent damage from spreading to additional components.

The receiver is of the superheterodyne type with an intermediate frequency of 70 MHz and a local oscillator frequency of 119.25 MHz. Its bandwidth is matched to the transmitted pulse. The RF and IF filters have a bandwidth of 6 MHz. The noise figure is about 1 dB. The receiver is both sensitive enough and quiet enough to easily detect solar and cosmic noise (Wilfong et al. 1993). In-phase (I) and quadrature (Q) components of the received signal referenced to a 70-MHz stable local oscillator (STALO) are provided to the data processing and control system for analysis. The STALO also generates the input pulse supplied to the transmitter by the TCU.

During transmit periods, a blanking signal is supplied by the control circuitry to block both local oscillators from the receiver to reduce saturation and recovery time of the sensitive receiver circuits. This enables the radar to operate to lower altitudes than might otherwise be possible.

c. The data processing and control system

The Data Processing and Control System has two major components: A Real-Time Processor (RTP) and a Data Analysis Processor (DAP). In addition to these major components, the control portion of the system contains Controller/Monitor Processors (CMPs), which interface antenna, transmitter, receiver, DAP, and peripherals to the RTP. The RTP consists of a number of custom cards on a VME bus. The RTP performs the following functions:

1) generates control signals for all CMPs,
2) receives and evaluates all status and monitoring signals from the CMPs,
3) controls the system receive/transmit timing and switching,
4) reduces the I and Q signals from the receiver to spectra that are supplied to the DAP,
5) removes ground clutter, and
6) provides communications links for the WWV receiver and Keyboard Display Unit (KDU).

The DAP provides the operator interface to the DRWP and converts the spectral data into wind speed and direction. It is hosted on a Digital Equipment Corporation MicroVAX computer and is connected to the KDU, a tape archive, a printer, and two modems that provide remote data access and control. It provides the capability for software development and maintenance, routine diagnostics and trouble-shooting, and retrieval of archived data.

d. Operating configurations

The KSC DRWP can be operated in a variety of configurations depending on the settings of a number of system parameters. In the configuration used to support routine operations, the first gate is set at 2011 m with a gate spacing of 150 m. An eight-bit pulse code is used. This results in 112 gates and a maximum altitude of 18 661 m. Altitudes approaching 25 km can be obtained with acceptable SNRs under certain conditions. The user may select the DELAY to the first range gate that determines the height of that gate. The GATE_SPACE parameter determines the spacing between gates and may be set as large as 600 m. A 1-, 2-, 4-, 8-, or 16-bit pulse CODE may be selected. The pulse code determines the maximum number of range gates permitted. The pulse WIDTH and repetition PERIOD are also user controllable. In its current operational configuration, the cycle time for the oblique beams is 5.5 min, which allows for the operational settings of the number of coherent and incoherent averages and the number of FFT points (288, 8, and 156, respectively, for the oblique beams and 624, 4, and 256, respectively, for the vertical beam).

The use of tailored combinations of parameters allows the radar to be used as a research instrument in addition to an operational one. The ability of the 50-MHz profiler to reach well into the stratosphere sets it apart from those operating at higher frequencies such as 449, 915, and 1215 MHz.

REFERENCES

Balsley, B. B., and K. S. Gage, 1982: On the use of radars for operational wind profiling. *Bull. Amer. Meteor. Soc.,* **63,** 1009–1018.

Barth, M. E., R. B. Chadwick, and D. W. van de Kamp, 1994: Data processing algorithms used by NOAA's wind profiler demonstration network. *Ann. Geophys.,* **12,** 518–528.

Carr, F. H., P. L. Spencer, C. A. Doswell III, and J. D. Powell, 1995: A comparison of two objective analysis techniques for profiler time-height data. *Mon. Wea. Rev.,* **123,** 2165–2180.

Clothiaux, E. E., R. S. Penc, D. W. Thomson, T. P. Ackerman, and S. R. Williams, 1994: A first-guess feature-based algorithm for

estimating wind speed in clear-air Doppler radar spectra. *J. Atmos. Oceanic Technol.,* **11,** 888–908.

Gage, K. S., and B. B. Balsley, 1978: Doppler radar probing of the clear atmosphere. *Bull. Amer. Meteor. Soc.,* **59,** 1074–1093.

Hidebrand, P. H., and R. S. Sekhon, 1974: Objective determination of the noise level in Doppler spectra. *J. Appl. Meteor.,* **13,** 808–811.

Jenkins, G. M., and D. G. Watts, 1968: *Spectral Analysis and Its Applications.* Holden Day, 525 pp.

May, P. T., 1993: Comparison of wind-profiler and radiosonde measurements in the Tropics. *J. Atmos. Oceanic Technol.,* **10,** 122–127.

——, and R. G. Strauch, 1989: An examination of wind profiler signal processing algorithms. *J. Atmos. Oceanic Technol.,* **6,** 731–735.

——, and ——, 1998: Reducing the effect of ground clutter on wind profiler velocity measurements. *J. Atmos. Oceanic Technol.,* **15,** 579–586.

Merceret, F. J., 1997: On rapid temporal changes of mid-tropospheric winds. *J. Appl. Meteor.,* **36,** 1567–1575.

——, 1998: Risk assessment consequences of the lognormal distribution of midtropospheric wind changes. *J. Spacecr. Rockets,* **35,** 111–112.

Miller, P. A., M. F. Barth, D. W. Van de Kamp, T. W. Schlatter, B. L. Weber, D. B. Wuertz, and K. A. Brewster, 1994: An evaluation of two automated quality control methods designed for use with hourly wind profiler data. *Ann. Geophys.,* **12,** 711–724.

Nastrom, G. D., and F. D. Eaton, 1995: Variations of winds and turbulence seen by the 50-MHz radar at White Sands Missile Range, New Mexico. *J. Appl. Meteor.,* **34,** 2135–2148.

Reiter, E. R., 1969: Structure of vertical wind profiles. *Radio Sci.,* **4,** 1133–1136.

Schumann, R. S., G. E. Taylor, S. A. Smith, and T. L. Wilfong, 1995: Application of a 50-MHz Doppler radar wind profiler to launch operations at Kennedy Space Center and Cape Canaveral Air Station. *Proc. 14th Conf. on Weather Analysis and Forecasting,* Dallas, TX, Amer. Meteor. Soc., 428–433.

Strauch, R. G., D. A. Merritt, K. P. Moran, K. B. Earnshaw, and D. van de Kamp, 1984: The Colorado wind profiling network. *J. Atmos. Oceanic Technol.,* **1,** 37–49.

Wakasugi, K. S. F., S. Kato, A. Mizutani, and M. Matsuo, 1985: Air and precipitation particle motions within a cold front measured by the MU VHF radar. *Radio Sci.,* **20,** 1123–1240.

Weber, B. L., and D. B. Wuertz, 1990: Comparison of rawinsonde and wind profiler measurements. *J. Atmos. Oceanic Technol.,* **7,** 157–174.

——, and ——, 1991: Quality control algorithm for profiler measurements of winds and temperatures. NOAA Tech. Memo. ERL WPL-212, 32 pp. [Available from NTIS, 5285 Port Royal Road, Springfield, VA 22161.]

——, and Coauthors, 1990: Preliminary evaluation of the first NOAA demonstration network wind profiler. *J. Atmos. Oceanic Technol.,* **7,** 909–918.

——, D. B. Wuertz, D. C. Law, A. S. Frisch, and J. M. Brown, 1992: Effects of small-scale vertical motion on radar measurements of wind and temperature profiles. *J. Atmos. Oceanic Technol.,* **9,** 193–209.

——, ——, D. C. Welsh, and R. McPeek, 1993: Quality controls for profiler measurements of winds and RASS temperatures. *J. Atmos. Oceanic Technol.,* **10,** 452–464.

Wilfong, T. L., S. A. Smith, and R. L. Creasy, 1993: High temporal resolution velocity estimates from a wind profiler. *J. Spacecr. Rockets,* **30,** 348–354.

——, ——, and C. L. Crosiar, 1997: Characteristics of high-resolution wind profiles derived from radar-tracked jimspheres and the ROSE processing program. *J. Atmos. Oceanic Technol.,* **14,** 318–325.

Wolfe, D., and Coauthors, 1995: An overview of the Mobile Profiler System: Preliminary results from field tests during the Los Angeles Free-Radical study. *Bull. Amer. Meteor. Soc.,* **76,** 523–534.

Woodman, R. F., 1985: Spectral moment estimation in MST radars. *Radio Sci.,* **20,** 1185–1195.

Wuertz, D. B., D. E. Wolfe, B. L. Weber, and R. B. Chadwick, 1995: NOAA's wind profiler demonstration network: An overview of applications and impact on research. NOAA Tech. Memo. ERL ETL-249, 29 pp. [Available from NTIS, 5285 Port Royal Road, Springfield, VA 22161.]

Yoe, J. G., and M. F. Larsen, 1992: VHF wind-profiler data quality and comparison of methods for deducing horizontal and vertical air motions in a mesoscale convective storm. *J. Atmos. Oceanic Technol.,* **9,** 713–727.